

Dynamic power and bandwidth allocation for DVB-based LEO satellite systems

Satya Chan¹ | Gyuseong Jo¹ | Sooyoung Kim¹ | Daesub Oh² | Bon-Jun Ku²

¹IT Convergence Research Center, Division of Electronics Engineering, Jeonbuk National University, Jeonju, Republic of Korea

²Radio and Satellite Research Division, ETRI, Daejeon, Republic of Korea

Correspondence

Sooyoung Kim, IT Convergence Research Center, Division of Electronics Engineering, Jeonbuk National University, Jeonju 54896, Republic of Korea.

Email: sookim@jbnu.ac.kr

Funding information

This research was supported by the Institute for Information and Communications Technology Promotion Grant funded by the Korea Government (MSIT, Development of the spectrum sharing technology for Non-GSO satellite system) under Grant 2021-0-00719.

Abstract

A low Earth orbit (LEO) satellite constellation could be used to provide network coverage for the entire globe. This study considers multi-beam frequency reuse in LEO satellite systems. In such a system, the channel is time-varying due to the fast movement of the satellite. This study proposes an efficient power and bandwidth allocation method that employs two linear machine learning algorithms and take channel conditions and traffic demand (TD) as input. With the aid of a simple linear system, the proposed scheme allows for the optimum allocation of resources under dynamic channel and TD conditions. Additionally, efficient projection schemes are added to the proposed method so that the provided capacity is best approximated to TD when TD exceeds the maximum allowable system capacity. The simulation results show that the proposed method outperforms existing methods.

KEYWORDS

LEO satellite, machine learning, multi-beam satellite, optimization, resource allocation

1 | INTRODUCTION

A low Earth orbit (LEO) satellite constellation enables seamless network coverage around the world, even in remote areas that cannot be reached by terrestrial networks, such as sea, desert, and forest regions [1]. Furthermore, LEO satellites outperform geostationary Earth orbit (GEO) satellites in terms of round-trip delay and free space loss, suggesting that a system based on LEO satellites could be a strong candidate for sixth-generation non-terrestrial networks. Therefore, the LEO satellite system has become a powerful tool enabling the use of the Internet of Things in the aforementioned remote areas [2, 3].

Modern satellites are capable of employing multi-beams with a frequency reusing scheme; for example,

each OneWeb satellite has 16 user beams, and each Starlink satellite has 8–32 configurable beams [1, 3]. Because of dynamic movement across the Earth's surface, the channel characteristics of a LEO satellite are more dynamic than those of a GEO satellite. This requires fast and efficient resource allocation (RA) for LEO systems to efficiently utilize limited power and bandwidth resources under dynamically changing constraints, including traffic demands (TDs) and channel conditions.

Another characteristic of modern satellite systems is the use of an adaptive coding and modulation (ACM) scheme to countermeasure time-varying channel impairments, including rain fading. ACM techniques equipped with multiple modulation and coding (MODCOD) modes have been specified in satellite standards such as digital video broadcasting via satellite second generation

(DVB-S2) and DVB-S2 extension (DVB-S2X) [4, 5]. Several commercial LEO satellite systems provide services using the techniques specified in the DVB-S2 or DVB-S2X [6].

Many studies have attempted to find optimum solutions to the RA problem for multi-beam satellite systems with ACM using either iterative convex optimization techniques or machine learning (ML)-based schemes [7–12]. One of these optimization methods has addressed power and bandwidth allocation for a multi-beam GEO satellite system using the Lagrange function, golden section theory, and subgradient iterations [8]. However, the simulation results showed that the maximum number of iterations to obtain the optimum solution for the satellite system with 10 beams could reach to 5000 iterations. With this many iterations, the optimization process can be an *NP-hard* problem for a time-varying channel and TD condition.

To minimize the energy consumption of ground users in the LEO satellite systems, another study proposed a computation offloading scheme, in which constraints were kept satisfied [11]. In that study, a non-convex objective function with constraints was converted into a well-known optimization problem called linear programming. As a result, there were five optimization steps aided by the primal-dual interior-point algorithm or a Matlab-based modeling system for convex optimization. Nevertheless, the complexity was still non-negligible, for example, it required at least 30 iterations to converge for 24 satellite beams, which is a heavy computation for LEO satellite systems.

Recently, a previous work presented a simple ML-based RA method for an integrated satellite and terrestrial network [7]. This work utilized two simple ML approaches, namely, the perceptron and linear regression (LR) method, followed by linear projection and a set of linear equations. The proposed scheme allocated the optimum bandwidth and power under time-varying TDs, and the simulation results demonstrated the superiority of the proposed scheme over existing methods in terms of power and spectral efficiencies. However, the proposed scheme was limited to a static channel condition for a GEO system. This implies that the efficiency of this scheme would be degraded for a LEO system with dynamic channel conditions.

With this background, we extend this previous study to the RA problem for multi-beam satellite systems under dynamic channels and TDs. To this end, we first establish a system model for an interference-limited LEO system with multi-beams and then present objective functions to solve the RA problem. Next, we derive a set of linear equations relating power and bandwidth by using Shannon's capacity equation. According to this relationship, power and bandwidth depend on each other, so we need to use an iterative searching method to determine the optimum value. To solve this problem, we divide the

process into several simple subsequent processes, including simple ML-based classification and LR tools. We also utilize an improved iterative projection tool to offer a manageable bit rate when the TD exceeds the system capacity. Most importantly, a proper projection technique should be applied under dynamic channel conditions. Because all operations applied to the proposed method are linear operations, the resulting complexity is very low.

The rest of this paper is organized as follows. Section 2 reviews related studies on RA schemes for multibeam satellite systems under interference-limited conditions. Section 3 first presents the interference-limited LEO system model using ACM and a set of linear equations to relate the signal-to-noise power ratio and bandwidth. Then, it proposes the computationally efficient RA algorithm with linear operations, followed by the projection scheme. Section 4 presents the performance evaluation results of the proposed method and compares them with the results of existing methods. Finally, Section 5 concludes the study.

2 | RELATED WORKS

RA methods for an integrated satellite and terrestrial system were proposed assuming that a multibeam satellite and terrestrial components reuse the total frequency bands of B (Hz) with a frequency reuse factor of N [7, 10]. For efficient RA under interference-limited conditions, the following objective function was formulated for a system with a frequency reuse factor of $N=3$, where three components (one satellite beam and two terrestrial cells) reuse each sub-band [10]:

$$\arg \min_{\mathbf{b}} \sum_i^N \{ \gamma_i^S + \gamma_i^{T_1} + \gamma_i^{T_2} \}, \text{ s.t. } \begin{cases} \sum_i^N b_i \leq B, \\ b_i \geq 0, \end{cases} \quad (1)$$

where $\gamma_i^S, \gamma_i^{T_1}$, and $\gamma_i^{T_2}$ denote the bit energy to noise spectral density ratio required at the satellite, first terrestrial cell, and second terrestrial cell, respectively, using the i th sub-band, b_i (Hz). In addition, $\mathbf{b} = [b_1 b_2 b_3]$ represents a bandwidth vector. This method typically produced invalid results of negative power or extremely large power when the TD was not within the system capacity, and it was impossible to find the existence of a valid solution before solving the optimization problem.

To solve this problem, the following modified objective function was proposed in [7]:

$$\arg \min_{\mathbf{b}} P_{\text{total}} \text{ s.t. } \sum_{i=1}^N b_i \leq B, b_i \geq 0, \quad (2)$$

where P_{total} (Watt) represents the total transmit power. In addition, the following power constraints were added to prevent invalid power allocation.

$$\begin{aligned} (P_t)_i^j &\geq 0, \forall i, j, \\ P_{\text{total}} &\leq P_{\text{max}}, \end{aligned} \quad (3)$$

where $(P_t)_i^j$ denotes the transmit power of the j th component using b_i and P_{max} denotes the maximum transmit power. Importantly, simple linear ML algorithms were combined to reduce the complexity of the RA process. However, the applicability of this algorithm was validated only for a GEO system with a static channel condition.

On the other hand, an optimal power optimal bandwidth (OPOB) method for a multibeam satellite system was proposed [8]. In this method, bandwidth and power resources are allocated so that the allocated capacity (bps) is most approximated to the TD using the following objective function:

$$\arg \min_{\mathbf{b}, \mathbf{p}} \sum_i^N \sum_j^{M_i} \left((R_b)_i^j - C_i^j \right)^2 \quad \text{s.t.} \quad \begin{aligned} \sum_i^N b_i &\leq B, \\ P_{\text{total}} &\leq P_{\text{max}}, \\ b_i &\geq 0, (P_t)_i^j &\geq 0, \end{aligned} \quad (4)$$

where M_i denotes the number of components using b_i , $(R_b)_i^j$ (bps) denotes a TD from the j th component using b_i , C_i^j (bps) denotes the capacity allocated to the j th component using b_i , and $\mathbf{p} = [(P_t)_1^1 \dots (P_t)_i^j \dots (P_t)_N^{M_N}]$ denotes the allocated transmit power vector. Based on the Shannon capacity bound, C_i^j could be estimated as follows:

$$C_i^j = b_i \log_2 \left(1 + \frac{(P_t)_i^j}{I_i^j + b_i N_0} \right), \quad (5)$$

where I_i^j represents the interference power at the j th component using f_i .

In the above OPOB scheme, the constrained objective function in (4) was transformed into an unconstrained one using non-negative Lagrange multipliers. Then, the optimum power and bandwidth were iteratively searched using a subgradient descent method, and the golden section theory was applied to avoid negative answers. Because of the objective function in (4), this method always produced optimum solutions even when the TD was greater than the maximum allowable capacity. However, this method required several iterations to find the solution. For example, our simulation results showed that it required 100 iterations for 16 satellite beams, indicating a high computational complexity for a LEO system.

3 | PROPOSED RESOURCE ALLOCATION METHODS FOR LEO SYSTEMS

3.1 | Interference-limited LEO satellite systems

Figure 1 illustrates the system configuration of multi-beam LEO satellites with a frequency reusing scheme. Each circle indicates a footprint of a satellite beam, and the color of each beam indicates the allocated frequency band. In this system, the frequency reuse factor is N , so N sub-bands are reused among the beams. As shown in the figure, the i th sub-band b_i (Hz), $1 \leq i \leq N$, has a center frequency f_i (Hz), $1 \leq i \leq N$. Let M_i be the number of beams using f_i ; then, by referring to the example in Figure 1, there are four beams using f_1 , so M_1 is 4, likewise $M_2 = 3$ and $M_N = 4$.

In the figure, examples of the desired signals are represented by solid line arrows, such as the signal receptions at beam j , $1 \leq j \leq 4$ using f_1 . Meanwhile, examples of the interference signals are presented by dashed line arrows, such as the interference at beam 2 using f_1 . Furthermore, $(P_t)_i^j$ and $(P_r)_i^j$ (Watt), respectively, denote the transmit and receive power at beam j , whereas $(G_t)_i^{k,j}$ and $(G_r)_i^{k,j}$, respectively, denote the transmit and receive antenna gains in the direction from beam k to beam j . Finally, $h_i^{k,j}$ indicates the channel gain across the path from beam k to beam j using f_i , and it includes path loss, rain attenuation, and other fading and losses.

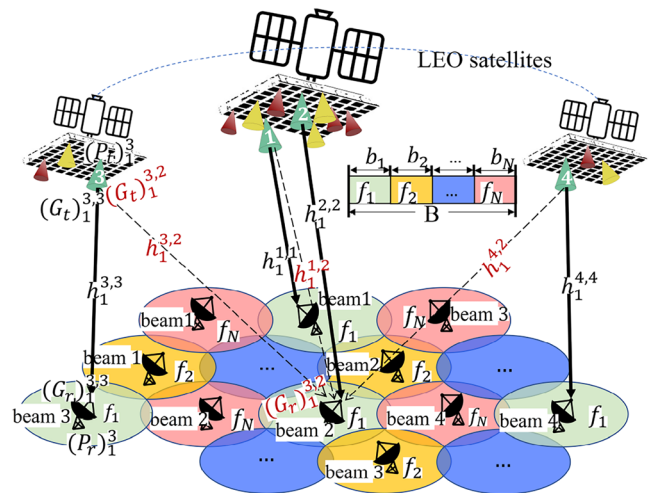


FIGURE 1 System model of LEO satellite

3.2 | Building a linear system with power and bandwidth

The purpose of this study is to allocate the optimum power and bandwidth resources, and they depend on each other by Shannon's capacity as follows:

$$\eta_i^j = (R_b)_i^j / b_i = \log_2(\text{SINR}_i^j + 1), \text{ (bps/Hz)} \quad (6)$$

where $(R_b)_i^j$ (bps) represents the TD from beam j using f_i and SINR_i^j represents the signal to interference plus noise power ratio at beam j using f_i . Therefore, we first develop a linear system with the allocated power, $(P_t)_i^j$, and bandwidth, b_i , as follows.

By assuming that there is no interference between beams using different sub-bands, we can construct a set of linear equations as follows [7]:

$$\Delta_i [\gamma_i^1 \gamma_i^2 \dots \gamma_i^{M_i}]^T = [1 \ 1 \dots 1]^T, \quad (7)$$

where γ_i^j denotes the bit energy to noise spectral density ratio, $(E_b)_i^j / N_0$ required at beam j using f_i , and

$$\Delta_i = \begin{bmatrix} 1/\rho_i^1 & -g_i^{2,1} \eta_i^2 & \dots & -g_i^{M_i,1} \eta_i^{M_i} \\ -g_i^{1,2} \eta_i^1 & 1/\rho_i^2 & \dots & -g_i^{M_i,2} \eta_i^{M_i} \\ \vdots & \vdots & \ddots & \vdots \\ -g_i^{1,M_i} \eta_i^1 & -g_i^{2,M_i} \eta_i^2 & \dots & 1/\rho_i^{M_i} \end{bmatrix}, \quad (8)$$

where ρ_i^j denotes the required bit energy to interference plus noise spectral density ratio, $(E_b)_i^j / ((I_0)_i^j + N_0)$ for beam j using f_i , and $(I_0)_i^j$ denotes the interference spectral density at beam j using f_i . Meanwhile, $g_i^{k,j}$ denotes the relative gain, which can be represented as follows:

$$g_i^{k,j} = \frac{(G_t)_i^{k,j} h_i^{k,j} (G_r)_i^{k,j}}{(G_t)_i^{k,k} h_i^{k,k} (G_r)_i^{k,k}}. \quad (9)$$

Solving (7) provides the optimum power allocation of $(P_t)_i^j$ with the following relationship with γ_i^j :

$$\begin{aligned} (P_t)_i^j &= \frac{(P_r)_i^j}{(G_t)_i^{j,j} h_i^{j,j} (G_r)_i^{j,j}} \\ &= \frac{(E_b)_i^j (R_b)_i^j}{(G_t)_i^{j,j} h_i^{j,j} (G_r)_i^{j,j}} = \frac{\gamma_i^j N_0 (R_b)_i^j}{(G_t)_i^{j,j} h_i^{j,j} (G_r)_i^{j,j}}. \end{aligned} \quad (10)$$

We note that the solution of (7) should be conditioned by ρ_i^j and η_i^j , as in (7) and (8). We convert the energy ratio of ρ_i^j into the power ratio to relate the power with bandwidth, which leads to the following equation:

$$\rho_i^j = \frac{(E_b)_i^j}{(I_0)_i^j + N_0} = \frac{(P_r)_i^j / (R_b)_i^j}{I_i^j / b_i + N_i / b_i} \quad (11)$$

where $I_i^j = (I_0)_i^j b_i$ and $N_i = N_0 b_i$ are the interference and noise powers at beam j using b_i , respectively. Therefore, (11) can be represented as follows:

$$\rho_i^j = \frac{(P_r)_i^j}{I_i^j + N_i} \cdot \frac{b_i}{(R_b)_i^j} = \frac{(P_t)_i^j (G_t)_i^{j,j} h_i^{j,j} (G_r)_i^{j,j}}{I_i^j + N_i} \cdot \frac{b_i}{(R_b)_i^j}. \quad (12)$$

We note that SINR_i^j in (6) is $(P_r)_i^j / (I_i^j + N_i)$; then, combining (6) and (12) leads to the following:

$$\rho_i^j = \left(2^{(R_b)_i^j / b_i} - 1\right) \frac{b_i}{(R_b)_i^j}. \quad (13)$$

The above (12) and (13) indicate that the value of ρ_i^j is associated with the power $(P_t)_i^j$ and the bandwidth b_i , so we need an iterative optimization tool or an exhaustive search to find the solution of (7). Therefore, the complexity is a concern. In addition, directly solving (7) can occasionally result in invalid solutions such as a negative power value; this typically occurs when the TD exceeds the system capacity.

3.3 | Linear operation-based intelligent resource allocation

The objective of this study is to find the solution of (2) and (3) for LEO systems in Figure 1. With the objective function of (2) and (3), we utilize the linear system of (7). Instead of running an exhaustive search of $(P_t)_i^j$ and b_i in (12) or iterative convex optimization algorithms to satisfy (2), the proposed method employs two simple ML-based linear tools, along with a linear projection tool. We refer to the proposed method as linear operation-based intelligent RA (LOIRA). Figure 2 illustrates the

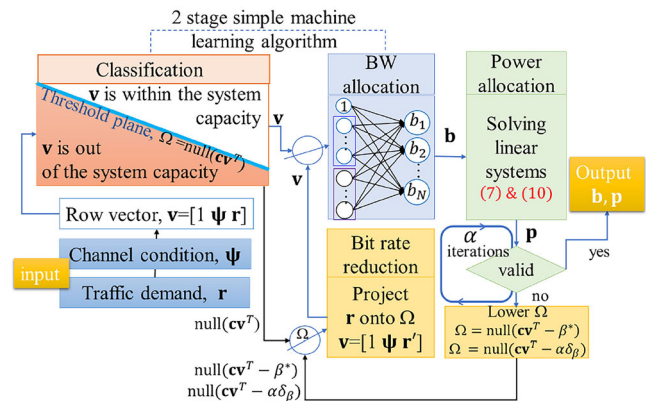


FIGURE 2 Operation of the LOIRA

operational principle of the LOIRA scheme, and the procedure is detailed in Algorithm 1.

Algorithm 1 Proposed bandwidth and power allocation algorithm

Input: $\mathbf{r}, \boldsymbol{\psi}$

Output: \mathbf{b}, \mathbf{p}

```

1:  $\mathbf{v} \leftarrow [1 \ \boldsymbol{\psi} \ \mathbf{r}]$ 
2:  $y \leftarrow \text{sgn}(\mathbf{c}\mathbf{v}^T)$  ▷ classification
3: if  $y = +1$  then
4:   go to 9
5: else ▷ projection
6:    $\mathbf{r}_p \leftarrow \text{Proj}_{\Omega}(\mathbf{r})$  with (21) and (23)
7:   REPLACING_TD( $\mathbf{r}_p$ )
8: end if
9: BP_ALLOCATION( $\mathbf{v}$ )
10:  $\alpha \leftarrow 1$ 
11: while  $(P_t)_i^j < 0, \forall i, j$  or  $P_{\text{total}} > P_{\text{max}}$  do
12:   case LOIRA 1
13:      $\mathbf{r}_p \leftarrow \text{Proj}_{\Omega_1}(\mathbf{r})$  with (28) and (29)
14:     REPLACING_TD( $\mathbf{r}_p$ )
15:     BP_ALLOCATION( $\mathbf{v}$ )
16:     go to 25
17:   case LOIRA 2
18:     if  $\alpha \delta_\beta \leq \beta^*$  then
19:        $\alpha \leftarrow \alpha + 1$ 
20:        $\mathbf{r}_p \leftarrow \text{Proj}_{\Omega_2}(\mathbf{r})$  with (31) and (32)
21:       REPLACING_TD( $\mathbf{r}_p$ )
22:       BP_ALLOCATION( $\mathbf{v}$ )
23:     end if
24: end while
25: End of allocation
26: produce  $\mathbf{b}$  and  $\mathbf{p}$ 
27:
28: function REPLACING_TD( $\mathbf{r}_p$ ) ▷ replacing  $\mathbf{r}$  with  $\mathbf{r}'$ 
29:    $(R'_b)_i^j \leftarrow \max[(r_p)_i^j, 0]$ 
30:    $\mathbf{r}' \leftarrow [(R'_b)_1^1 \dots (R'_b)_1^{M_1} \ (R'_b)_2^1 \dots (R'_b)_N^{M_N}]$ 
31:    $\mathbf{v} \leftarrow [1 \ \boldsymbol{\psi} \ \mathbf{r}']$ 
32: end function
33:
34: function BP_ALLOCATION( $\mathbf{v}$ )
35:    $\mathbf{b}^T \leftarrow \mathbf{W}_{\text{lin}} \mathbf{v}^T$  ▷ bandwidth allocation
36:   Estimate  $\mathbf{p}$  using (7) and (10) ▷ power allocation
37: end function

```

The LOIRA has an input vector \mathbf{v} :

$$\mathbf{v} = [1 \ \boldsymbol{\psi} \ \mathbf{r}], \quad (14)$$

where $\boldsymbol{\psi}$ and \mathbf{r} denote row vectors with the elements of channel conditions and TDs for all beams, respectively, as follows:

$$\boldsymbol{\psi} = [\psi_1^{1,1} \ \psi_1^{1,2} \ \dots \ \psi_1^{1,M_1} \ \dots \ \psi_1^{M_1,M_1} \ \psi_2^{1,1} \ \dots \ \psi_N^{M_N,M_N}], \quad (15)$$

where $\psi_i^{k,j} = (G_t)_i^{k,j} h_i^{k,j} (G_r)_i^{k,j}$, and

$$\mathbf{r} = \left[(R_b)_1^1 \ (R_b)_1^2 \ \dots \ (R_b)_1^{M_1} \ (R_b)_2^1 \ \dots \ (R_b)_N^{M_N} \right]. \quad (16)$$

As output, the LOIRA produces the allocated power and bandwidth vectors \mathbf{b} and \mathbf{p} as follows:

$$\mathbf{b} = [b_1 \ b_2 \ \dots \ b_N], \quad (17)$$

and

$$\mathbf{p} = \left[(P_t)_1^1 \ (P_t)_1^2 \ \dots \ (P_t)_1^{M_1} \ (P_t)_2^1 \ \dots \ (P_t)_N^{M_N} \right]. \quad (18)$$

Referring to Figure 2, along with Algorithm 1, we detail the operational process of the LOIRA as follows. Below, the line numbers inside parentheses indicate line numbers in Algorithm 1. Upon receiving the input vector \mathbf{v} at the resource allocation center (line 1), the LOIRA method activates the linear classification tool, that is, the *perceptron* (line 2), which classifies whether the solution of (7) for \mathbf{v} satisfies the conditions given in (3), to avoid expending unnecessary effort. If $y = +1$, it means that the result will satisfy the condition given in (3) (line 3). Otherwise, that is, $y = -1$, which is the opposite case and means that \mathbf{r} is beyond the maximum allowable system capacity under the current channel condition, $\boldsymbol{\psi}$. Then, the LOIRA method activates the linear projection tool to replace \mathbf{r} with \mathbf{r}' inside \mathbf{v} (lines 5–8). Detailed descriptions of the projection with the perceptron will be given in the following Section 3.4.

Afterward, bandwidth and power are estimated (line 9). First, \mathbf{v} goes through the LR tool to find \mathbf{b} as follows (line 35):

$$\mathbf{b}^T = [b_1 \ b_2 \ \dots \ b_N]^T = \mathbf{W}_{\text{lin}} \mathbf{v}^T, \quad (19)$$

where \mathbf{W}_{lin} denotes the weight matrix of the LR. The weight values are trained using a supervised learning process before the system implementation, and they can be regularly updated. In other words, they are trained using the datasets determined to produce valid \mathbf{b} and \mathbf{p} from the exhaustive search. Next, \mathbf{p} is estimated using (7) and (10) (line 36).

Finally, the estimated \mathbf{p} is tested to determine whether it satisfies the condition given in (3) (line 11). If \mathbf{p} satisfies the condition, the LOIRA method produces its estimated results of \mathbf{b} and \mathbf{p} and finishes the allocation process (lines 25–26). On the other hand, if \mathbf{p} does not satisfy the condition because of a false-positive error

caused by the classifier (line 11), additional projections are required. For this, we propose two types of iterative projection schemes, namely, LOIRA 1 and 2. In the case that the system is determined to use LOIRA 1 (line 12), one more projection is allowed (line 13). Afterward, \mathbf{r} is replaced with \mathbf{r}' (line 14), and \mathbf{b} and \mathbf{p} are reallocated (line 15). On the other hand, the system using LOIRA 2 allows multiple projections until the result satisfies (3) or the maximum number of iterations is reached (lines 18–23). The details of this multiple projection procedure are explained in the last paragraph of Section 3.4. Although iterative projections can be made, the LOIRA method generally runs only a few iterations, as the preceding classification tool predetermines the labels.

3.4 | Projection-based traffic demand regulation within the system capacity

The classifier in Figure 2 estimates its output y using the following well-known linear equation (line 2).

$$y = \text{sgn}(\mathbf{c}\mathbf{v}^T) = \text{sgn}(c_0 + \mathbf{c}_\psi\boldsymbol{\Psi}^T + \mathbf{c}_r\mathbf{r}^T), \quad (20)$$

where $\mathbf{c} = [c_0 \mathbf{c}_\psi \mathbf{c}_r]$ represents the pre-trained weight vector. We note that the datasets for training \mathbf{c} are produced through RA using LR, followed by (7), (10), and (3) before the system implementation, and \mathbf{c} can be regularly updated. Because the output y value can be either +1 or -1, the threshold space of the classifier will be the solution space of $\mathbf{c}\mathbf{v}^T = 0$, that is, the null space of $\mathbf{c}\mathbf{v}^T$.

When \mathbf{v} is in the -1 region, we need to regulate \mathbf{r} to push \mathbf{v} into +1 region. We note that \mathbf{v} will lie in the -1 region when \mathbf{r} is too large under the given $\boldsymbol{\Psi}$. In this case, the regulation should be specifically performed to reduce \mathbf{r} while minimizing the reduction amount. This can be achieved by reducing \mathbf{r} by projecting it onto the threshold space. Keeping in mind that the classification is made by \mathbf{v} instead of \mathbf{r} , the threshold space exists for $\mathbf{c}\mathbf{v}^T$ but not $\mathbf{c}_r\mathbf{r}^T$.

Therefore, we need to draw the null space of $\mathbf{c}_r\mathbf{r}^T$ from $\mathbf{c}\mathbf{v}^T$. To this end, we first let

$$\boldsymbol{\Omega} = \text{null}(\mathbf{c}\mathbf{v}^T). \quad (21)$$

Next, we separate the null space of $\mathbf{c}_r\mathbf{r}^T$ from $\boldsymbol{\Omega}$ as follows:

$$\boldsymbol{\Omega} = \boldsymbol{\Lambda} + \mathbf{a}_\psi, \quad (22)$$

where $\boldsymbol{\Lambda} = \text{null}(\mathbf{c}_r\mathbf{r}^T)$, and \mathbf{a}_ψ is a vector translating from the subspace $\boldsymbol{\Lambda}$ to the affine subspace $\boldsymbol{\Omega}$ [13]. In other words,

$$\mathbf{a}_\psi = \text{null}(\mathbf{c}\mathbf{v}^T) - \text{null}(\mathbf{c}_r\mathbf{r}^T). \quad (23)$$

Because the target of regulation is only on \mathbf{r} and not on $\boldsymbol{\Psi}$, which represents the channel condition, we can treat $\boldsymbol{\Psi}$ as a constant vector during the projection process.

Eventually, the reduction of \mathbf{r} can be performed by projecting it onto $\boldsymbol{\Omega}$, and this can be performed by projecting $\mathbf{r} - \mathbf{a}_\psi$ onto $\boldsymbol{\Lambda}$ and then translating the result back as follows (line 6):

$$\begin{aligned} \mathbf{r}_p &= \text{Proj}_{\boldsymbol{\Omega}}(\mathbf{r}) = \text{Proj}_{\boldsymbol{\Lambda}}(\mathbf{r} - \mathbf{a}_\psi) + \mathbf{a}_\psi \\ &= \mathbf{A}(\mathbf{A}^T\mathbf{A})^{-1}\mathbf{A}^T(\mathbf{r} - \mathbf{a}_\psi) + \mathbf{a}_\psi, \end{aligned} \quad (24)$$

where $\mathbf{r}_p = [(r_p)_1^1 (r_p)_1^2 \dots (r_p)_1^{M_1} (r_p)_2^1 \dots (r_p)_N^{M_N}]$.

To avoid a negative bit rate, the final result of the projection tool is represented as follows (line 7, i.e., lines 28–32):

$$\mathbf{r}' = \left[(R'_b)_1^1 (R'_b)_1^2 \dots (R'_b)_1^{M_1} (R'_b)_2^1 \dots (R'_b)_N^{M_N} \right], \quad (25)$$

where $(R'_b)_i^j = \max[(r_p)_i^j, 0]$. In addition, the matrix \mathbf{A} is a standard matrix for the projection, and its column vectors are the basis vectors of $\boldsymbol{\Lambda}$ as follows:

$$\mathbf{A} = [\mathbf{x}_1 \mathbf{x}_2 \dots \mathbf{x}_L], \quad (26)$$

and

$$\boldsymbol{\Lambda} = \lambda_1\mathbf{x}_1 + \lambda_2\mathbf{x}_2 + \dots + \lambda_L\mathbf{x}_L, \quad (27)$$

where $\lambda_i \in \mathbb{R}$, $1 \leq i \leq L$. We note that L represents the dimension of $\boldsymbol{\Lambda}$, and $L = \dim(R^n) - 1$ when \mathbf{r} represents a vector in (R^n) . This is because $\boldsymbol{\Lambda}$ is a hyperplane, that is, an orthogonal complement of \mathbf{r} , that is, $\boldsymbol{\Lambda} = \mathbf{r}^\perp$. Note that the complexity of calculating $\mathbf{A}(\mathbf{A}^T\mathbf{A})^{-1}\mathbf{A}^T$ does not affect the complexity of the proposed method. This is because \mathbf{A} only depends on \mathbf{c}_r and can be pre-estimated before the system operation.

However, \mathbf{r}' can cause an invalid result because of an error by the perceptron. Therefore, the LOIRA method employs two types of iterative projection methods: LOIRA 1 and LOIRA 2. LOIRA 1 is equipped with a fixed margin value to lower the threshold, which guarantees no false-positive error. As a result, only one more projection is permitted. Therefore, \mathbf{r} is projected onto the $\text{null}(\mathbf{c}\mathbf{v}^T - \beta^*)$, where β^* represents the minimum positive value that makes the classification using $\text{sgn}(\mathbf{c}\mathbf{v}^T - \beta^*)$ produce no false-positive error.

In other words, $\text{null}(\mathbf{c}\mathbf{v}^T - \beta^*)$ can be considered a lowered threshold space for \mathbf{v} , that is

$$\Omega_1 = \text{null}(\mathbf{c}\mathbf{v}^T - \beta^*) = \Lambda + \mathbf{a}_{\psi_1}. \quad (28)$$

The value of β^* could be found by running the exhaustive search over the datasets used to train the perceptron, and the vector translating from subspace Λ to Ω_1 is estimated as follows:

$$\mathbf{a}_{\psi_1} = \text{null}(\mathbf{c}\mathbf{v}^T - \beta^*) - \text{null}(\mathbf{c}_r\mathbf{r}^T). \quad (29)$$

Then, the additional projection can be performed using the above Ω_1 (line 13):

$$\mathbf{r}_p = \text{Proj}_{\Omega_1}(\mathbf{r}). \quad (30)$$

With this additional projection, the replacement of \mathbf{r} with \mathbf{r}' is made (line 14), followed by the bandwidth and power allocation (line 15).

Although LOIRA 1 mostly guarantees valid outputs, the TD reduction can be excessive for some value of \mathbf{r} . To improve the spectral efficiency, LOIRA 2 increases the margin values of $\alpha\delta_\beta$, where α and δ_β , respectively, denote the number of iterations and the increment of margin. The maximum number of iterations is limited by the condition, $0 < \alpha\delta_\beta \leq \beta^*$. With LOIRA 2, iterative projection followed by RA is performed by lowering the threshold space until the allocated \mathbf{p} satisfies the condition (line 11) or the maximum number of iterations is reached. For this, we set the projection space as follows:

$$\Omega_2 = \text{null}(\mathbf{c}\mathbf{v}^T - \alpha\delta_\beta) = \Lambda + \mathbf{a}_{\psi_2}, \quad (31)$$

and the vector translating from subspace Λ to Ω_2 is estimated as follows:

$$\mathbf{a}_{\psi_2} = \text{null}(\mathbf{c}\mathbf{v}^T - \alpha\delta_\beta) - \text{null}(\mathbf{c}_r\mathbf{r}^T). \quad (32)$$

Finally, the projection can be performed using the above Ω_2 (line 20):

$$\mathbf{r}_p = \text{Proj}_{\Omega_2}(\mathbf{r}). \quad (33)$$

After every projection, the replacement of \mathbf{r} with \mathbf{r}' is made (line 21), followed by the bandwidth and power allocation (line 22).

4 | SIMULATION RESULT

The evaluation is performed on the basis of three aspects: average transmit power, average capacity per beam, and the number of iterations, as in shown in Figures 3 to 6. The simulation is performed over a compact LEO satellite system to shorten the huge simulation

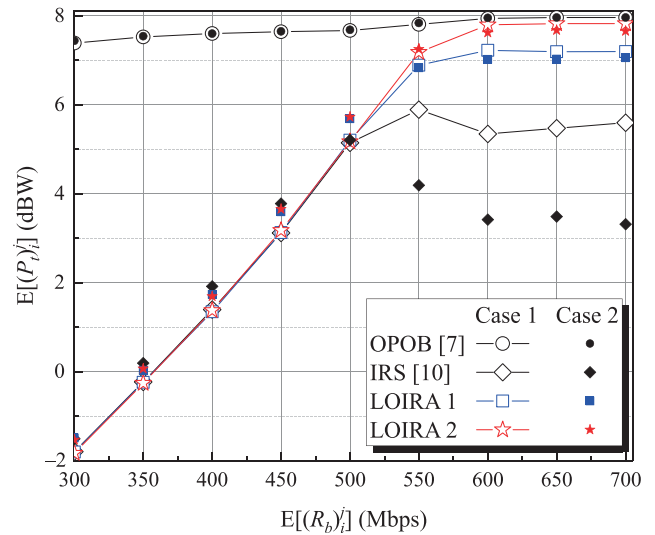


FIGURE 3 Comparison of average transmit power (dBW)

time. It is assumed that RA is performed for 16 LEO satellite beams, with the frequency reuse factor $N = 4$ and $M_i = M = 4, 1 \leq i \leq 4$. We consider a LEO system compatible with existing systems such as Telesat, OneWeb, and SpaceX LEO systems [14]. The system has an altitude of 1200 km, and B and P_{\max} are set to 1 GHz and 20 dBW, respectively. The center frequency is assumed to be 18.5 GHz, and the antenna gains of the satellite and Earth station are set to be 31.8 dBi and 43.5 dBi, respectively. To adapt to the attenuation and interference in the system, the MODCOD schemes defined in the DVB-S2X are used as ACM schemes [5].

The time-varying channel conditions of the system are simulated with a dynamic channel gain of ψ_i^{kj} , and it is assumed to be a Gaussian random variable with the following mean values.

$$E[\psi_i^{kj}] = \begin{cases} -115\text{dB}, j = k. \\ -130\text{dB}, j \neq k. \end{cases} \quad (34)$$

In addition, two different cases, that is, Case 1 and Case 2 with variance values of 0.25 and 2 in dB^2 scale, are used to evaluate the performance of the algorithm with dynamic channel conditions. Furthermore, TD, $(R_b)_i^j$ is also assumed to be a Gaussian random variable with a standard deviation, $\sigma = 100$ Mbps, $(R_b)_i^j \geq 0$. The simulation was performed by varying the mean value of TD, $E[(R_b)_i^j] = [300, 700]$ (Mbps). Lastly, the increment in the margin δ_β in LOIRA 2 was set to $0.2\beta^*$.

For the comparison, we used two conventional methods. First, the OPOB method in [8] was implemented using the interior-point algorithm built in Matlab. Second, the intelligent resource allocation (IRS) method in [7] was applied.

Figure 3 depicts the average transmit power per beam, $E[(P_t)_i^j]$, for the different RA methods: When $E[(R_b)_i^j] \leq 500$ Mbps, the transmit powers of the IRS, LOIRA 1, and LOIRA 2 are almost the same, because most of the TDs are within the capacity of the system. Notably, these methods require less power in Case 1 when the channel variance of Case 1 is smaller than that of Case 2. When $550 \leq E[(R_b)_i^j] \leq 600$, the power required by IRS decreases because it cannot properly adapt to the channel dynamics, especially in Case 2. When $E[(R_b)_i^j] \geq 600$, the power required by IRS, LOIRA 1, and LOIRA 2 do not change by $E[(R_b)_i^j]$ because TDs are generally above the system capacity. When $E[(R_b)_i^j] \geq 500$, LOIRA 2 requires the highest power among the above three methods. Smaller power requirements indicate larger differences between the TD and provided capacity. For example, when $E[(R_b)_i^j] \geq 600$, LOIRA 1 requires 0.5 dB less power than LOIRA 2, and the IRS requires another 2 dB less power than LOIRA 1. This eventually leads to IRS having the smallest capacity provision of the IRS among the investigated methods, which can be confirmed in the following Figure 4.

Finally, the OPOB requires the highest power among the entire range investigated because it does not utilize the linear system in (7) to minimize power; it requires 1 dB to 9 dB more power than LOIRA 2 when $E[(R_b)_i^j] \leq 500$. Alternatively, the results from Case 2 prove that LOIRA 1 and 2 require less power compared with the IRS while providing the same capacity when TDs are under the system capacity.

Figure 4 proves the capacity enhancements of LOIRA 1 and 2 compared the conventional schemes. As long as TDs remain within the system capacity, the capacities of all investigated methods keep increasing as TDs increase. On the other hand, LOIRA 1 and 2 outperform the other existing methods in terms of capacity. Among these, IRS provides the smallest capacity. Although the OPOB provides slightly higher capacity than LOIRA 2, it consumes excessive power, as depicted in Figure 3.

As described above, there is a trade-off between the provided capacity and power consumption. For a relative comparison, Figure 5 compares $E[(P_t)_i^j]$ versus average achievable spectral efficiency per beam, $E[\eta_i^j]$. From the figure, IRS requires up to 1 dB more power than LOIRA 1 and 2 at the same $E[\eta_i^j]$ even though LOIRA 1 and 2 both require more power than IRS at the same TD in Figure 3. Importantly, the maximum $E[\eta_i^j]$ of IRS is limited because it does not reflect dynamic channel gain. The transmit powers of the OPOB are almost constant across the investigated $E[\eta_i^j]$ values.

In summary, the OPOB achieves the maximum capacity, but its power efficiency is low, especially when TD is lower than the system capacity. However, IRS and the proposed LOIRA use the minimum power

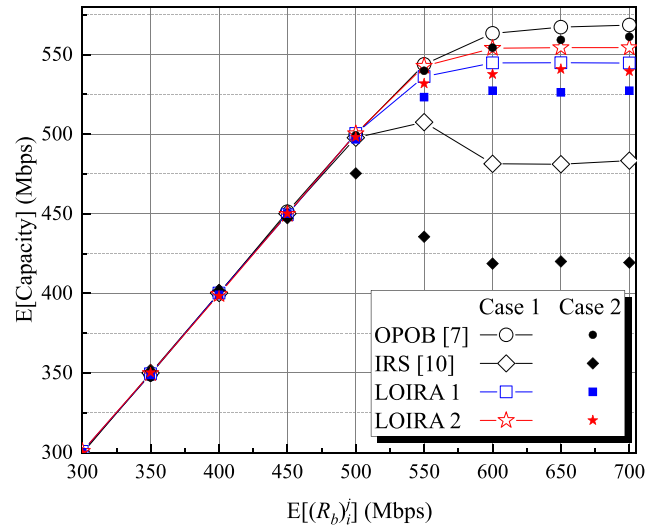


FIGURE 4 Comparison of the average capacity

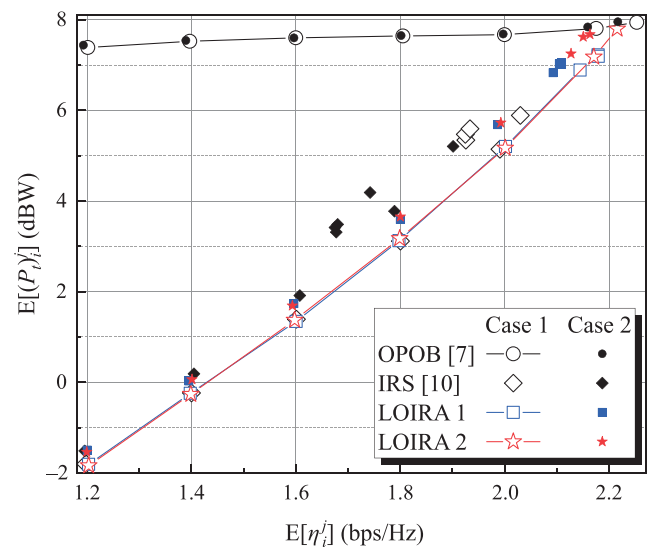


FIGURE 5 Spectral efficiency versus transmit power

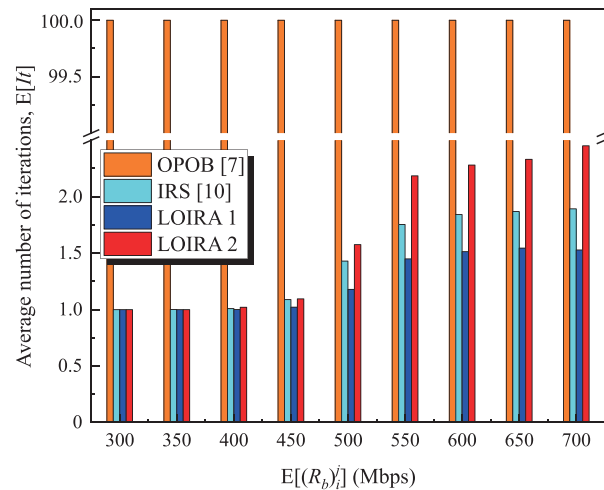


FIGURE 6 Comparison of average number of iterations

TABLE 1 Number of multiplications

Estimation	OPOB [8]	IRS [7]	LOIRA
Power	$(It)(N)\left(\frac{M^3}{3} + \frac{3M^2}{2} + \frac{25M}{6}\right)$	$(It)(N)\left(\frac{M^3}{3} + \frac{3M^2}{2} + \frac{13M}{6}\right)$	$(It)(N)\left(\frac{M^3}{3} + \frac{3M^2}{2} + \frac{13M}{6}\right)$
Bandwidth	$(It)(n_{bi})(N)(M^2 + 32M)$	$(It)(N^2)(M)$	$(It)(N^2)(M^2 + M)$
Dual variables	$2(It)$	-	-
Projection	-	$(It)(N^2)(M^2)$	$(It)(N)(M^2)(N + 1)$
Perceptron	-	$(N)(M)$	$(N)(M^2 + M)$

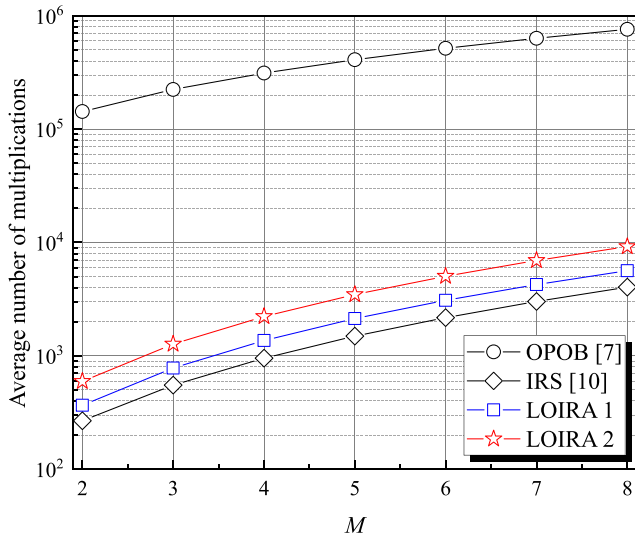


FIGURE 7 Complexity comparison in terms of the average number of multiplications

when the TD is affordable within the system capacity, indicating a high increase in power efficiency. If the channel dynamics become high, the IRS shows its limitation to allocate proper resources. Alternatively, the proposed LOIRA efficiently finds the optimum power and bandwidth.

For the complexity comparison, we first investigate the average number of iterations, $E[It]$, required for each method under Case 2, and Figure 6 shows the results. The OPOB requires $E[It]$ of 100 regardless of $E[(R_b)_i^j]$, and this is 50 times greater than that of LOIRA 2. When the TDs are within the system capacity, that is, when almost no projection is required, the IRS, LOIRA 1, and LOIRA 2 require only one iteration on average. This can be investigated when $E[(R_b)_i^j] \leq 450$. On the other hand, LOIRA 2 requires slightly more iterations than IRS and LOIRA 1, with at most one more iteration on average, if TDs are increasing.

Table 1 compares the complexity of each algorithm in terms of the number of the multiplications by assuming $M = M_1 = M_2 = \dots = M_N$. We note that the perceptron in IRS and LOIRA operates only at the first iteration. In the

table, It represents the number of iterations investigated in Figure 6. In addition, n_{bi} represents the number of iterations to find the bandwidth allocation for the OPOB method, which requires an iterative approach to solve a nonlinear equation. Figure 7 compares the average number of multiplications according to M when $N = 4$. We found that the average number of multiplications of LOIRA is in the same complexity order as that of the IRS method, that is, LOIRA 1 and 2 require 1.5 and 2 times more multiplications than IRS. However, OPOB is 100 times more complex than LOIRA. This investigation reveals that the total complexity is strongly dependent on the number of iterations, as shown in Figure 6.

5 | CONCLUSION

In this study, we have extended a previous study on the RA algorithm with two linear ML tools to LEO satellite systems. Because the channel and TD are dynamic, they are used as input to the ML tools. The proposed method has been demonstrated to be able to identify the optimum solution using only a few iterations because it can predict whether the TD would be within the system capacity using a simple perceptron. In addition, the complex RA problem has been divided into two steps: bandwidth allocation using the LR tool and power allocation by solving linear equations. Moreover, two different types of projection schemes are applied, namely, LOIRA 1 and LOIRA 2, which are tailored for LEO systems. LOIRA 2 enables multiple projections with increasing margins to the threshold space, which avoids the false-positive error from the perceptron. The simulation results show that the proposed method highly enhances power and spectral efficiency compared with conventional schemes, especially when the dynamics of channel condition changes highly. The simulation results in this study considered the gross effect of channel dynamics as if all the channel impairments are integrated into a single parameter. In the future, this study will be extended by applying the proposed method to realistic mobile LEO satellite channels, including various channel impairments such as Doppler shift.

CONFLICT OF INTEREST

The authors declare that there are no conflicts of interest.

ORCID

Satya Chan  <https://orcid.org/0000-0002-9146-6177>

REFERENCES

1. S. Xia, Q. Jiang, C. Zou, and G. Li, *Beam coverage comparison of LEO satellite systems based on user diversification*, *IEEE Access* **7** (2019), 181656–181667.
2. S. Jung, G. Im, D. Jung, P. Kim, J. Ryu, and J. Kang, *Performance analysis of DSSS- and CSS-based physical layer for IoT transmission over LEO satellites*, *ETRI J.* **44** (2022), no. 4, 543–559.
3. X. Lin, S. Cioni, G. Charbit, N. Chuberre, S. Hellsten, and J. Boutillon, *On the path to 6G: embracing the next wave of low earth orbit satellite access*, *IEEE Commun. Mag.* **59** (2021), no. 12, 36–42.
4. ETSI EN 302 307, Digital Video Broadcasting (DVB); Second generation framing structure, channel coding and modulation systems for Broadcasting, Interactive Services, News Gathering and other broadband satellite applications (DVB-S2), 2013.
5. ETSI - EN 302 307-2 V1.2.1, Digital Video Broadcasting (DVB); Second generation framing structure, channel coding and modulation systems for Broadcasting, Interactive Services, News Gathering and other broadband satellite applications; Part 2: DVB-S2 Extensions (DVB-S2X), 2020.
6. S. Chen, S. Sun, and S. Kang, *System integration of terrestrial mobile communication and satellite communication—the trends, challenges and key technologies in 5G and 6G*, *China Commun.* **17** (2020), no. 12, 156–171.
7. S. Chan, H. Lee, S. Kim, and D. Oh, *Intelligent low complexity resource allocation method for integrated satellite-terrestrial systems*, *IEEE Wirel. Commun. Lett.* **11** (2022), no. 5, 1087–1091.
8. M. Jia, X. Zhang, X. Gu, Q. Guo, Y. Li, and P. Lin, *Interbeam interference constrained resource allocation for shared spectrum multibeam satellite communication systems*, *IEEE Int. Things J.* **6** (2019), no. 4, 6052–6059.
9. O. Kodheli, N. Maturo, S. Chatzinotas, S. Andrenacci, and F. Zimmer, *NB-IoT via LEO satellites: an efficient resource allocation strategy for uplink data transmission*, *IEEE Int. Things J.* **9** (2022), no. 7, 5094–5107.
10. U. Park, H. Kim, D. Oh, and B.-J. Ku, *Interference-limited dynamic resource management for an integrated satellite-terrestrial system*, *ETRI J.* **36** (2014), 519–527.
11. Q. Tang, Z. Fei, B. Li, and Z. Han, *Computation offloading in LEO satellite networks with hybrid cloud and edge computing*, *IEEE Int. Things J.* **8** (2021), no. 11, 9164–9176.
12. D. Zhou, M. Sheng, Y. Wang, J. Li, and Z. Han, *Machine learning-based resource allocation in satellite networks supporting internet of remote things*, *IEEE Trans. Wirel. Commun.* **20** (2021), no. 10, 6606–6621.
13. R. Piziak and P. L. Odell, *Affine projections*, *Comput. Math. Appl.* **48** (2004), no. 1, 177–190.
14. I. del Portillo Barrios, B. Cameron, and E. Crawley, *A technical comparison of three low earth orbit satellite constellation systems to provide global broadband*, *Acta Astronautica* **159** (2019), 123–135.

AUTHOR BIOGRAPHIES



Satya Chan received his BTech degree in electronics engineering from NPIC, Cambodia, in 2014. Right after he graduated, he worked as a voluntary staff in an NGO from 2014 to 2017 and worked as a reporter at AE company for 7 months. He received his ME degree from Jeonbuk National University, Republic of Korea, in 2019, and currently, he is pursuing his PhD degree at the same university. His research interests include satellite communications and standardization, physical layer security for MIMO systems, soft detection for coded MIMO systems, and error correction coding.



Gyuseong Jo received his BS degree in electronics engineering from Jeonbuk National University, Jeonju, Republic of Korea, in 2022, and currently, he is pursuing his ME degree at the same university. His research interests are satellite and mobile communications.



Sooyoung Kim received her BS degree in electrical and electronics engineering from Korea Advanced Institute of Science and Technology, Korea, in 1990. After working in the Satellite Communication Technology Division, Electronics and Telecommunications Research Institute (ETRI), Republic of Korea, from February 1990 to September 1991, she received her MSc and PhD degrees in electrical and electronics engineering from University of Surrey, UK, in 1992 and 1995, respectively. From November 1994 to June 1996, she was employed as a research fellow at the Centre for Satellite Engineering Research, University of Surrey, UK. In 1996, she re-joined the Satellite Communication Technology Division, ETRI, Republic of Korea, and worked as a team leader until February 2004 to develop efficient transmission techniques for digital satellite communication systems. She is now a professor at Jeonbuk National University. Her research interests include coded MIMO schemes, forward error correction coding, physical layer security schemes, and satellite communications. She is actively working on Working Party 4B of ITU-R for standardization activities for satellite communications, and she has been appointed as an international standardization expert in Korea. She has published

more than 100 technical papers in the field of wireless/satellite communications. She has been a Technical Program Committee member at various conferences and an editorial board member of the *International Journal of Satellite Communications and Networking*.



Daesub Oh received his PhD degree from Jeonbuk National university in 2014. He has been working for Electronics and Telecommunications Research Institute (ETRI) since 2000. His research interests are in the broad areas of satellite communication, wireless communication, and spectrum management.



Bon-Jun Ku received his PhD degree from Chungbuk National University in 2010. Since 1999, he has worked for Electronics and Telecommunications Research Institute (ETRI). He is currently a principal member of the research staff at the

Radio and Satellite Research Division in ETRI. His research interests include satellite communications systems, high-altitude platform stations, and wireless communication system engineering.

How to cite this article: S. Chan, G. Jo, S. Kim, D. Oh, and B.-J. Ku, *Dynamic power and bandwidth allocation for DVB-based LEO satellite systems*, ETRI Journal **44** (2022), 955–965. <https://doi.org/10.4218/etrij.2022-0192>